Research Article | Vol. 29, No. 11 / 24 May 2021 / Optics Express 16087
Optics EXPRESS

Impact of industrial environments on visible light communication

DANIEL SCHNEIDER,[1,*] ABHIJEET SHROTRI,[2] HOLGER FLATT,[1] OLIVER STÜBBE,[2] ALEXANDER WOLF,[3] ROLAND LACHMAYER,[3] AND CHRISTIAN-ALEXANDER BUNGE[4]

[1]*Fraunhofer IOSB, Branch Industrial Automation (IOSB-INA), Campusallee 1, D- 32657 Lemgo, Germany*
[2]*Technische Hochschule Ostwestfalen-Lippe, Campusallee 12, D- 32657 Lemgo, Germany*
[3]*Leibniz Universität Hannover, Institute of Product Development (IPeG), An der Universität 1, D- 30823 Garbsen, Germany*
[4]*Hochschule für Technik, Wirtschaft und Kultur (HTWK) Leipzig, Fakultät für Digitale Transformation, Zschochersche Str. 69, D- 04229 Leipzig, Germany*
[*]*daniel.schneider@iosb-ina.fraunhofer.de*

Abstract: Visible-light communication is a promising technology for industrial environments. However, a variety of physical effects may influence the communication quality in this potentially harsh environment: Dust and other particles lead to increased attenuation. Artificial light sources and industrial processes, such as grinding and welding, cause optical cross-talk. A multitude of reflective surfaces can lead to fading due to multi-path propagation. These three aspects are experimentally investigated in exemplary manufacturing processes at five different production sites in order to estimate the relative importance and their specific impact on VLC transmission in industrial areas. Spectral measurements demonstrate the presence of interfering light sources, which occupy broad parts of the visible spectrum. They give rise to flickering noise, which comprises a set of frequencies in the electrical domain. The impact of these effects on the communication is analysed with reference to the maximum achievable channel capacity and data rate approximation based on on-off keying is deduced. It is found that cross-talk by environmental and artificial light sources is one of the strongest effects, which influences the optical, but also the electrical spectrum. It is also observed that industrial areas differ strongly and must be categorised according to the manufacturing processes, which can induce quite a variation of dust and attenuation accordingly.

1. Introduction

Visible light communication (VLC) is one approach to solve the radio spectrum crunch. In industrial applications, field devices increasingly operate at temporary locations or completely mobile via wireless links. The number of mobile applications and devices rise, whereas the available radio bandwidth remains the same [1]. As a result of the increasing spectrum usage, a wireless connection can ultimately be lost, leading to an overall denial of service [2]. In contrast, a mobile industrial production system requires field devices to be as reliable as wired devices (relating to availability, ruggedness, scalability). The development of mobile communication technologies like the current standard 5G or Software Defined Radio poses technologies which shall efficiently distribute the available spectrum. However an even broader spectrum becomes available when using the visible part of the electromagnetic spectrum. Originally focusing on infra-red communication in 2003, the Visible Light Communications Consortium (VLCC) was founded in Japan with the intent to use the visible spectrum for standardized communication [3]. Worldwide a growing interest emerged, leading, for example, to the research project "HOME Gigabit Access" (OMEGA) in VLC-based consumer networks in Europe [4]. In the consumer and office sector, ceiling and office lamps are also used as transceivers for communication as

#421757 https://doi.org/10.1364/OE.421757
Journal © 2021 Received 10 Feb 2021; revised 6 Apr 2021; accepted 12 Apr 2021; published 11 May 2021

Optics EXPRESS

well as illumination. Mobile terminals can receive data within the cone of light [4–6]. In the back-haul branch, a satellite or ground station uses VLC to transmit aggregated mobile data for instance by using highly directional lasers [7]. Lately, VLC is also used for implementing indoor navigation systems in shopping malls [8,9].

Though proven as a potent communication technology, VLC struggles with the application in industrial environments [10]. The industrial environment is different from office, home and laboratory environments. For example, a VLC system placed in a robotic production cell exhibits Ethernet frame latencies varying from 0.1 ms up to 0.8 s, due to probable communication loss [11]. The particle influence as well as the channel characteristics are named as primary performance limitations [12]. Signal degradation caused by artificial light sources, multi-path propagation, shadowing and mobility are amongst the most important hindrances [5,6,13,14]. Those are nevertheless normal conditions in industrial environments. However, the occurrence of these effects and their respective impact on an optical communication system is currently unclear.

In this contribution, a comprehensive view on the degrading physical effects on the optical signals in industrial environments is presented. The focus of this paper lies on physical measurements and data analysis, whereas their impact on communication properties are deduced, exposing degradation in the channel capacity, the bit-error probability and achievable data rate. In order to model individual degrading effects, a novel method to decompose superimposed light in spatially, spectral measurements is derived. The studied impacting factors are analysed to assess their potential influence on VLC in industrial areas. Thus, the influences of industrial environments are modelled to assess the VLC-system parameters such as the data rate of the overall system. Here, it becomes apparent that industries can vary greatly and must be categorized.

The article is structured as follows: In Section 2 the industrial environment is introduced and an explanation of the degrading effects is given. In the following Section 3, a model is derived which allows to estimate the respective impact on the communication performance. In Section 4 the method, results and analysis of the measurements are demonstrated. A discussion of the measurement results is conducted in Section 5, followed by a conclusion in Section 6.

2. Visible-light communication in industrial areas

The considered VLC system consists of an LED transmitter at the ceiling of a workshop and a photo detector as a receiver, which is placed near the ground. It is possible by the same means to reverse the communication direction, but here primarily the down-link connection is surveyed. This connection can be influenced by nearby machines, which act as a source of reflections (multi-path propagation). Production processes like welding and grinding or artificial light sources lead to interfering stray light or attenuating particles. An overview of this industrial scenario is sketched in Fig. 1.

Each degrading effect has been empirically analysed at five different production sites, which will be explained subsequently. Among the five examined production sites the environment has an average area of 1000 m^2. The average ceiling height is 5 m with the illumination installed at 4 m distance to the floor.

2.1. Dust and particles in the optical path

Whereas outdoor free-space optical communication systems must overcome the scattering effects e.g. by fog and rain, for instance covered by Rajbhandari and Ghassemlooy [2,15], scattering effects in indoor industrial environments are more diverse. Fabrication and processing often produces dust particles, which will lead to additional attenuation and may alter the optical spectrum. In the context of losses due to dust particles in industrial areas, scattering will be the predominant effect. An electromagnetic wave with the initial intensity I_0 is attenuated on its optical path with length s by particles who scatter and absorb the electromagnetic wave. The

Optics EXPRESS

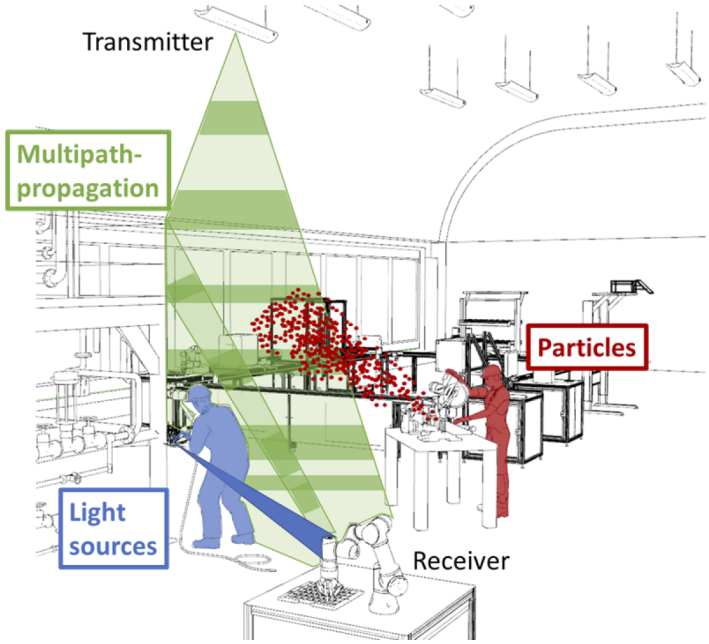

Fig. 1. Overview of the VLC communication within an industrial environment. Interfering effects such as attenuating particles, stray light and multi path propagation are indicated in colours.

attenuation follows the Lambert-Beers law [16]:

$$I(s) = I_0 \cdot \mathrm{e}^{-\alpha \cdot s} \tag{1}$$

with the attenuation coefficient α. The type of scattering – and thus the attenuation and its wavelength dependence – is determined by the relative diameter d_s of the particles with respect to the wavelength λ.

- $d_s \leq \lambda$: **Rayleigh scattering** decreases rapidly with increasing wavelength according to $\alpha \propto \lambda^{-4}$ [17].
- $d_s \approx \lambda$: **Mie scattering** shows no particular wavelength dependence, $\alpha \neq f(\lambda)$ [18].
- - $d_s > \lambda$: **Geometrical optics** describe the light path directly in terms of attenuation, independent of the wavelength [19].

To further determine the attenuation and scattering, further information are necessary, such as the molecular composition, shape, size distribution or the relative cross section of the particles in the light beam. In the surveyed companies primarily metal is being processed, therefore the charted, supplemental information of metal grinding processing is used [20]. The particle concentration, is however currently mostly uncharted for common industrial environments and for particle producing processes (e. g. soldering) and is therefore measured. The particles range in the diameter between 1-10 *mu*m. The particles have a mostly spherical shape [20] and consist mainly of elemental carbon [21]. The typical particle size d_s in industrial areas can therefore be assumed to be larger than λ so that geometrical optics can be applied. In this case, the attenuation

Optics EXPRESS

coefficient depends on the number of particles N_p per volume and their size as follows [21]:

$$\alpha = N_p \cdot \pi \left(\frac{d_s}{2}\right)^2 . \tag{2}$$

Thus, larger particles as well as higher particle densities lead to stronger attenuation.

2.2. Environmental light sources

The transmission of a signal, which is modulated onto a light wave, is also subject to these environmental (artificial or natural) light sources. Grinding, welding and other manufacturing processes produce incandescent light (like sparks or flames) which interfere with the optical signal. In addition, in industrial environments different lighting conditions are present like digital signalling, human machine interfaces or at light emitting processes like welding. Hence, several different sources of light have been investigated, especially the sun as a major contributor to background radiation [22]. This can be described as an additive irradiation, which can saturate the receiver. In addition to the optical spectrum, the light sources are found to be time varying and thus exhibit an electrical spectrum (the time varying, electrically modulated signal on the optical wave) after demodulation by a photo-detector. This effect can be described by an additional frequency-dependent electrical noise signal so that particular frequencies are more compromised than others. Artificial light sources like fluorescent lights have been found to exhibit this behaviour [23,24]. But these degrading effects are commonly subsumed as additive white noise on the signal, neglecting the dynamic behaviour, location and spectral distribution [25]. Thus, the optical as well the electrical spectral density of these interfering signals determine the actual impact on the signal transmission and should be identified. However, the optical irradiation distribution as well as the frequency-dependent flickering behavior is currently mostly unidentified and needs to be measured.

2.3. Reflective surfaces

Due to the often metallic surfaces of machines and inventory an incident light is reflected. This leads to more than one possible path the signal can take from the transmitter to the receiver. In this so-called multi-path scenario, several parts of the optical signal arrive at different times at the receiver, thus with different losses and time delays. The frequency response of such a multi-path transmission forms a low-pass filter that restricts the available channel bandwidth. The radio-based multi-path propagation has been exhaustively researched [26–28] and has led to the ITU standardization of several models for mobile communication, in particular the tapped-delay line (TDL) model [29]. This approach superimposes weighed time-delayed copies of the transmitted signals in the electrical domain. The ITU uses the TDL model for different speed scenarios (pedestrian, car, train). VLC relies on an incoherent channel so that multi-path propagation will only affect the modulated signal (in the electrical domain), but does not lead to carrier fading. Theoretically, the impulse-response can be calculated based on the exact knowledge of each reflective element in the environment [30]. Besides the different channel model, the current VLC standard IEEE 802.15.7 only includes a roaming concept, whereas the multi-path properties and physical effects of industrial environments are ignored. In order to further assess the impact on the optical communication the TDL parameters need to be measured.

The above mentioned effects (particle attenuation, multi-path propagation, interfering light) form the most occurring and therefore important influences on the optical signal in the surveyed industrial sites.

3. Impact on the communication channel

The respective impact of physical effects needs to be examined to assess their impact on the optical communication channel. This VLC channel is hereafter modelled according to Fig. 2,

Optics EXPRESS

incorporating all named effects into one model. Based on this model the information capacity and the data rate (parameter bit error probability) for a non-return-to-zero transmission is derived.

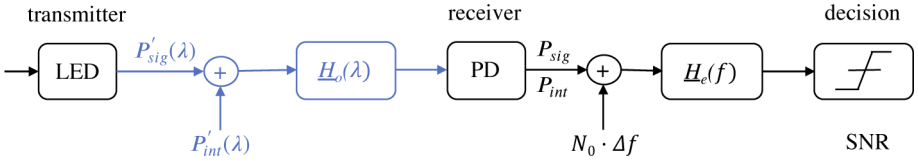

Fig. 2. Model of the VLC channel with the optical path in blue and the electrical in black. The optical spectral densities of the signal $P'_{sig}(\lambda)$ and the interfering element $P'_{int}(\lambda)$ are assumed to add incoherently, will be transformed into an electrical signal at the photo-diode. The optical filter $\underline{H}_o(\lambda)$ includes the wavelength-dependent attenuation and the opto-electrical conversion of the photo-diode and is assumed to be identical for the two optical components. The electrical filter $\underline{H}_e(f)$ accounts for the bandwidth limitation Δf of the circuitry and for the reduction of noise with spectral density of N_0.

3.1. Information capacity

The information capacity is the maximum amount of information that can pass through a communication channel without an error. According to Shannon [31], the maximum information capacity C_{max} increases linearly with the available bandwidth B and logarithmic with the signal-noise ratio (SNR) due the possibility to encode more bits per symbol. If the SNR varies with the frequency, the total capacity can be estimated by dividing the total bandwidth into frequency intervals of constant SNR and integrate:

$$C_{max} = \int_0^B \log_2 \left[1 + SNR(f)\right] \mathrm{d}f. \tag{3}$$

The studied environmental effects have an impact on the signal power due to attenuation, but will also affect the transmission by interfering cross-talk. This interfering signal is unknown and is assumed to be random. Therefore, it will be treated as an additional noise term using the signal-interference-plus-noise ratio $SINR$ instead of the SNR in Eq. (3), which can be expressed as:

$$SNR(f) \approx SINR(f) = \frac{P'_{sig}(f)}{P'_{int}(f) + N_0} \tag{4}$$

with the spectral power density of the signal $P'_{sig}(f)$, the interfering signal $P'_{int}(f)$ and the average noise power density N_0, which is assumed to be white thermal noise. In contrast to the well-known definition of the SNR, this expression is not based on the total power of the entire signal or the interference, but on the frequency-dependent spectral power densities. This is indicated by the prime. The thermal-noise density in Eq. (4) is defined by the Johnson-Nyquist relation

$$N_0 = 4k_B T, \tag{5}$$

with the Boltzmann constant k_B and the temperature T. Other noise sources (e. g. shot noise or other radiation sources) contribute to the minimal thermal noise at room temperature ($T = 290\,\mathrm{K}$, $N_0 = 4 \cdot 10^{-18}\,\mathrm{W/Hz}$) depending on the receiver design. In order to factor this uncertainty in, it is assumed that N_0 varies by the factor 1000. The noise density N_0 therefore ranges between $4 \cdot 10^{-18}\,\mathrm{W/Hz}$ and $4 \cdot 10^{-15}\,\mathrm{W/Hz}$. Note that these quantities of the SNR are evaluated as electrical signals within the receiver circuit. Furthermore, the two domains of an electrically modulated signal on the one hand and the used optical light wave on the other hand have to be incorporated. It is assumed that the emitted optical wavelength band is entirely dependent on the

Optics EXPRESS

light source and its characteristics. The power of the emitted signal is dependent on the electrical modulation. Based on these assumptions, the optical and the electrical spectrum can be evaluated separately from each other. As shown in the modelling approach in Fig. 2 the received signal in the optical domain is dependent on the optical power density P' and the optical channel $\underline{H}_o(\lambda)$. For this study, the optical signal and the interfering signal are assumed to propagate similar paths with almost identical optical properties $\underline{H}_o(\lambda)$. The received current of the signal and interfering signal at the photo-diode with responsivity $\Re$ can thus be expressed as:

$$i_{sig} = \Re \cdot \int_{\lambda} P'_{sig}(\lambda)|\underline{H}_o(\lambda)|^2 \mathrm{d}\lambda \tag{6}$$

$$i_{int} = \Re \cdot \int_{\lambda} P'_{int}(\lambda)|\underline{H}_o(\lambda)|^2 \mathrm{d}\lambda. \tag{7}$$

The electrically converted optical powers can be estimated assuming a constant resistance R_{PD} of the photo-diode:

$$P_{sig} = i_{sig}^2 \cdot R_{PD} \tag{8}$$

$$P_{int} = i_{int}^2 \cdot R_{PD}. \tag{9}$$

The Eqs. (8) and 9 give an estimate over the integral powers, but no indication on their frequency dependence within the electrical spectrum. The electrical spectrum of the signal $\underline{S}_{sig}(f)$ and interference $\underline{S}_{int}(f)$ are assumed to be normalised ($\int_{-\infty}^{+\infty} |\underline{S}(f)|^2 \mathrm{d}f = 1$) so that the spectral densities can be expressed by their spectral densities after electrical filtering with $\underline{H}_e(f)$ with the weighing factors obtained from Eqs. (8) and 9 as

$$P'_{sig}(f) = P_{sig} \cdot |\underline{H}_e(f)\underline{S}_{sig}(f)|^2 \tag{10}$$

$$P'_{int}(f) = P_{int} \cdot |\underline{H}_e(f)\underline{S}_{int}(f)|^2. \tag{11}$$

Using Eqs. (4), 10 and 11, the signal-to-noise ratio at the decision (Fig. 2) can be described as

$$SNR(f) \approx \frac{P_{sig}}{P_{int}} \cdot \frac{|\underline{S}_{sig}(f)|^2}{|\underline{S}_{int}(f)|^2 + \frac{N_0}{P_{int}}}. \tag{12}$$

Furthermore, reflective surfaces lead to multi-path propagation, where the signal reaches the receiver via different paths with individual delays. The above stated model allows the estimation of multi-path propagation also. This effect leads to a distortion, which can be modelled by a simple tapped-delay approach (see also Fig. 12). In a linear, time invariant system (LTI), an emitted signal $x(t)$ passes through a channel which is received as $y(t)$ [32]

$$y(t) = \int_{-\infty}^{\infty} x(t-\tau) \cdot h(\tau)\, d\tau, \tag{13}$$

which is characterised by the channel impulse response $h(\tau)$. If the received signal consists of L discrete multi-path components, where the k^{th} component is attenuated by α_k and delayed by τ_k [32], the channel impulse response becomes

$$h(t) = \sum_{k=1}^{L} \alpha_k \cdot \delta(t - \tau_k), \tag{14}$$

with the corresponding frequency response

$$\underline{H}_e(f) = \sum_{k=1}^{L} \alpha_k \cdot e^{-\jmath 2\pi f \tau_k}. \tag{15}$$

The attenuation and the delay spread (the temporal broadening of the impulse response due to different propagation delays) is specific for an environment. The superposition of the exponential

Optics EXPRESS

functions lead to a frequency selectivity with fades, which limits the available bandwidth. Inserting Eq. (15) in Eq. (10) allows for the calculation of the adjusted *SNR* in Eq. (12), thus factoring in all found physical effects in one novel model. Inserting Eq. (12) into Eq. (3) results the theoretical channel capacity of the link under different environmental conditions.

Table 1. Tapped delay channel model for a static and a mobile industrial environment of an impulse response

	Static		Mobile	
Tap k	τ_k	α_k	τ_k	α_k
1	0 ns	0 dB	0 ns	0 dB
2	23 ns	−3.9 dB	23 ns	−4.3 dB
3	44 ns	−4.7 dB	46 ns	−6.0 dB
4	98 ns	−9.0 dB	82 ns	−8.4 dB
5	148 ns	−9.3 dB	156 ns	−10.4 dB

3.2. Non-return-to-zero transmission characteristics

The derivation above gives a rough estimate on the theoretically achievable capacity. In many applications, however, typical transmission schemes are used which achieve only a fraction of this theoretical limit. Often, the on-off keying (OOK) non-return-to-zero (NRZ) is used as a transmission format because of its simplicity. For an estimate, it is hereafter assumed that a typical transmitter and receiver hold a bandwidth of $B = 50\,\text{MHz}$ and ideally reaches a maximum bit rate of $R_b = 100\,\text{Mbit/s}$ based on OOK-NRZ. For such a transmission scheme, the bit-error probability can be estimated as [32]:

$$BER_{NRZ} = \frac{1}{2}\text{erfc}\left(\frac{1}{2\sqrt{2}}\sqrt{\frac{P_{sig}}{N_0 \cdot \Delta f}}\right), \tag{16}$$

where the signal power P_{sig} is considered in the electrical domain according to Eq. (8) and $\Delta f \leq B$ is the noise bandwidth, which is restricted by the matched filter at the receiver. The signal power P_{sig} decreases with optical attenuation, whereas the noise power $N_0 \cdot \Delta f$ increases with the data rate R_b. In the analysis, ideal Nyquist pulses are assumed such that $\Delta f = \frac{R_B}{2}$. Thus, for a given signal power and noise spectral density, a maximum bit rate can be found such that a required bit-error probability can be achieved, e. g. compliant the the IEEE 802 Ethernet Standard $BER_{NRZ} = 10^{-9}$. For the subsequent investigations, we assume a maximum $BER = 10^{-9}$ corresponding to a signal-to-noise ratio of $SNR \geq 21.6\,\text{dB}$.

4. Measurement and analysis of influencing optical effects

In the following section, the method for measuring the above stated effects is explained. The respective measurement results are demonstrated and their impact on the communication capability is assessed. For a specific assessment of the influences on a VLC-system, some assumptions are made according to typical components in VLC systems. According to EN 12464-1 [33], a minimum illumination of 300 lx is required in industrial indoor work places, which we consider within this publication. This photometric property can be transformed into a minimum intensity of interfering signals about $I = 2.1\,\text{W/m}^2$ (visible range). It can further be assumed that the light has a non-orthogonal incidence upon the receiver (additionally not fully modulated). Therefore, an intensity of $1\,\text{W/m}^2$ is considered throughout the study. The bandwidth of the transmitter and receiver is further assumed to be 50 MHz and the active area of the detector is assumed to be $A_{PD} = 4\,\text{mm}^2$.

Optics EXPRESS

4.1. Attenuation due to dust

To estimate the particle influence on an optical path, information about the particle densities are necessary. The locations of the measurement are chosen in such a way that the measuring device can be placed in the close vicinity of the processes (e. g. welding, grinding, soldering machine) and additionally at random locations. In order to measure the particle concentrations, a particle analyzer is employed (HoldPeak HP-5800F). It detects the average concentrations of particles ranging up to 2.5 µm and up to 10 µm sized particles, which for calculation purposes are assumed to have the diameter 2.5 µm and 10 µm, leading to a view on a worst case scenario. The median and the standard deviation is calculated for a respective set of 10 measurements. The particle density varies from environment to environment up to factor 10, as can be observed in Fig. 3. For general assessment on the influence of dust on the communication channel it is important to distinguish between industries that involve large amounts of dust particles or not. Another important aspect is the form of applied air filtering and ventilation. Measurements show that for soldering alone the particle density can be reduced by more than a factor of ten with ventilation. The dust from metal cutting can increase the particle density be another two orders of magnitude. Particles with a diameter of 2.5 µm are averagely present with a density of 5.6 µg/m^3 whereas 10 µm particles are present with a density of 6.8 µg/m^3. In comparison, a soldering process has been measured in close proximity (0.2 m distance) with an active ventilation, which exhibits densities of 75 µg/m^3 (2.5 µm) and 95 µg/m^3 (10 µm). While soldering without ventilation shows average particle densities of 710 µg/m^3 and 1990 µg/m^3. In order to estimate the impact on a light based signal, the corresponding particle concentrations N_p are calculated and translated into the combined attenuation per m according to Eq. (2) in Fig. 3. The attenuation ranges between 0.002 dB/m and 70 dB/m. These processes, however, seem to be extremes. The five investigated companies exhibited relatively similar particle densities, which on average lead to almost negligible additional attenuation.

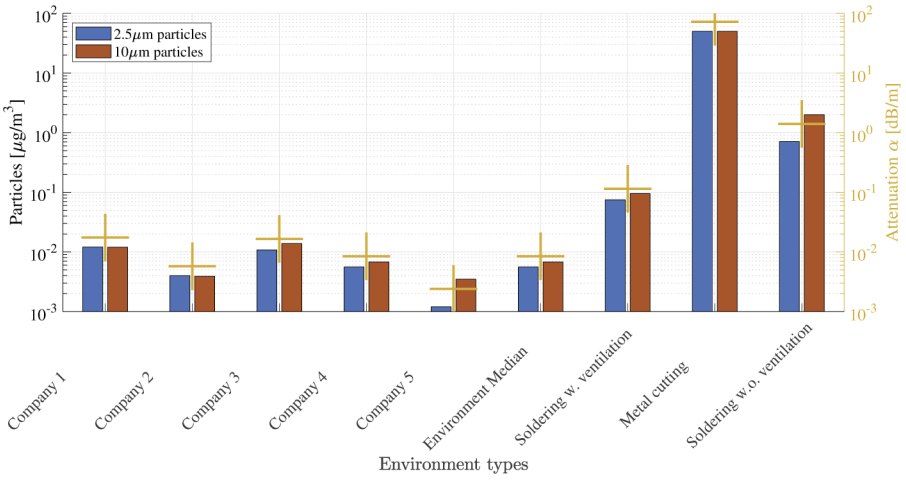

Fig. 3. Measured, environmental particle densities at different sites and processes, respective with the combined attenuation.

This attenuation reduces the signal power and thus the maximum transmission capacity. In this case the only interfering effect is the increased attenuation due to dust so the interference term in Eq. (12) becomes zero and the equation simplifies to

$$SNR(f) \approx \frac{P_{sig}}{N_0} |\underline{S}_{sig}(f)|^2. \tag{17}$$

Optics EXPRESS

Here, the electrical signal power P_{sig} is derived from Eqs. (6) and 8, which is proportional to I^2 and decreases with the optical attenuation $\alpha(\lambda)$ according to Eq. (1). Thus the *SNR* and the total capacity depend on λ and on the particle concentration:

$$C_{max} \approx \int_0^B \log_2\left(1 + \frac{P_{sig}(\lambda)}{N_0}|\underline{S}_{sig}(f)|^2\right) df. \tag{18}$$

Figure 4 shows the impact of additional attenuation due to dust on the achievable information rate C_{max} under the above stated assumptions (4 m distance) and different noise levels N_0 within the receiver. The additional attenuation due to dust affects the maximum information rate moderately. The initial capacity of about 1.8 Gbit/s decreases to about 600 Mbit/s for an additional attenuation of 30 dB. If the specific OOK-NRZ modulation is used, the influence of dust becomes even more pronounced. For an attenuation in excess of 20 dB, the achievable data rate is limited to well below 1 Mbit/s and drops in several cases even below 1 kbit/s (Fig. 4 on the right). In the ideal case of $N_0 = 4 \cdot 10^{-18}\,\frac{\mathrm{W}}{\mathrm{Hz}}$, the dust does not affect the data rate till the attenuation is larger then 7 dB. For more noisy receivers, the data-rate reduction sets in even earlier. This shows that only industries that involve metal cutting, soldering without ventilation or other quite dusty processes prohibit a high data-rate VLC, whereas in all studied companies the attenuation by particles had only a minor effect.

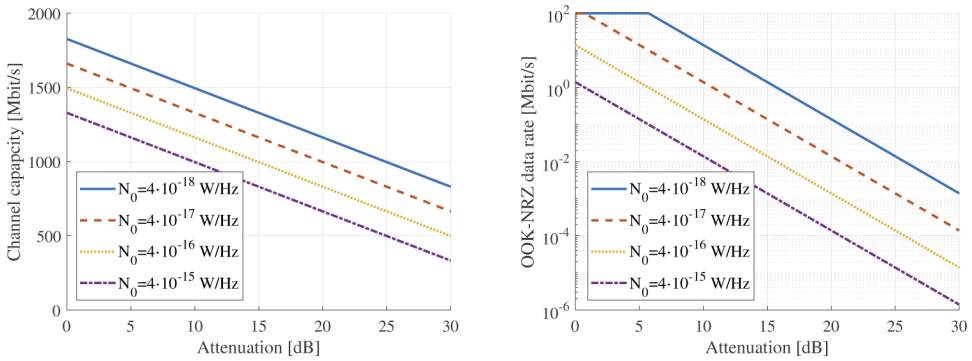

Fig. 4. Simulation results of the reduction of the maximum information capacity (left) and the achievable bit rate for OOK-NRZ transmission (right) for $BER \leq 10^{-9}$ at different noise spectral densities within the receiver.

4.2. *Environmental sources of light*

In order to ascertain what kind of irradiation and spectral occupation exists in the industrial environment these properties need to be measured. Usually, light sources are measured in a dark room with no other influences. In order to obtain the light properties in industrial environments, however, isolating the light sources is an unsuitable method, especially when a production process emits light (e. g. automated welding). Considering that light sources have angle-dependent radiation characteristics, the orientation and field of view of the spectrometer highly affects the measurement quality by changing the proportions of the superimposed light sources [25]. Therefore, a spectrometer (the spectrometer plots the spectrum of each measured point separately as a graph of wavelength on abscissa and absolute irradiance on ordinate (OceanInsight FLAME)) is rotated on two controlled axes (Skywatcher Acuter AZ Merlin) allowing the detection of the different positions of light sources while factoring out angular dependencies. This approach allows for the detection of spatially distributed light sources as well as their classification. Previous studies also suggest the measurement setup to be carried out at positions of visible

Optics EXPRESS

highlighting [25]. Spots of visible highlighting are for example beside machinery or at illuminated workplaces. This method of location selection results in the measurement (the measurement has been set up in a way, that the spectrometer (field of vision = 60°) is moved on a hemisphere in steps of 20° azimuth and 10° elevation). of the maximum irradiance sources and will therefore be used.

4.2.1. Measurement algorithm for spatially superimposed sources

A drawback of the measurement outside a darkroom is the superposition of several light sources on a taken measurement. In order to identify the individual source contributions, a novel, recursive method is introduced in the pseudo code Algorithm 1. This uses the fact that different light sources cannot be in one place, but must be localized besides each other. Assuming that alignment maximizes the measured irradiance an individual light source can be found when the total irradiance progress reaches a maximum. Therefore, at first the total irradiance is calculated for each measurement, while local maxima in relation to neighboring positions are calculated. These positions are considered possible origins of light sources. Next, the respective visible spectrum (380-780 nm) at the irradiation maximum is normalized and the spectral maxima and minima are evaluated, forming a specific pattern. It is detected whether this pattern fits to other already known spectra e. g. to the spectrum of the sun (ASTM G173-03: Direct + circumsolar Reference Spectra). Once the spectrum is known, the respective pattern is subtracted from the data and the local irradiation is calculated anew. If the spectrum is not known, the pattern needs to be evaluated. Neighboring measurements must have the same pattern, but with a proportional lower intensity. Hence the gradient field around the local irradiance maximum is calculated. All steady maxima belong to the identified source, while unsteady maxima are erased from the pattern. This process is repeated until all measured irradiance values are explained by a pattern. The method is validated by reference to dark room measurements of three exemplary light sources (fluorescent light, white LED, UV light). It is however possible that the irradiance distribution of a source measured by the method deviates from dark room measurement of the same. This deviation has two possible reasons: Although a good isolation can be achieved by the orientation alignment, still some superposition of second sources may occur, which is however not harmful as it still represents a really occurring portion of the spectral occupation. Furthermore aging can affect the sources. After several years of operating time for instance an LED emits a different spectrum than the same new LED. To factor this variation in all leftover irradiation is summarized in a rest model, which can be treated as an offset.

4.2.2. Flickering measurement

Furthermore, there exists a large variety of flickering light sources in industrial environments, caused by artificial illumination or manufacturing processes. Therefore, the flicker of the environment is measured in order to find relevant occupied signal frequencies $\underline{S}_{sig}(f)$. The measurement setup (the measurements are conducted at the same locations as the spectrum measurements to find out the flickering frequencies of disturbing light sources) for flickering measurements includes a detection circuit of a photo-diode (Osram BPX65) and a trans-impedance amplifier. The photo-diode is mounted with a band pass optical filter (Thorlabs FESH0800) to eliminate the wavelengths outside of visible light spectrum. The output of trans-impedance amplifier is evaluated using an oscilloscope (Keysight MSO9254A) to get the spectrum information. Furthermore, special processes like welding and grinding are observed in a semi-darkened environment to get the specific, environmental free flicker (the spectrum and flicker of the environment is measured before the process starts and is subtracted from the latter measurement data).

Optics EXPRESS

Algorithm 1 Decomposition of superimposed light measurements

```
for Every measurement position do
    for Every measurement orientation do
        Calculate total irradiance
    end for
    for Each local irradiance maximum do
        Normalize spectrum
        Create a pattern of local maxima and minima
        Compare pattern to known patterns
        if Pattern is known then
            Subtract pattern from measurements
        else
            Calculate gradient field of local maxima and minima in neighboring orientations
            if Gradients steady then
                Create new model from pattern
            else
                Neglect unsteady maxima in the pattern
                Create new model from reduced pattern
            end if
        end if
    end for
end for
```

4.2.3. Analysis of environmental light sources

In Fig. 5, the median of the whole measurement set at one location as well as the maximum values of the used spherical measurement are shown. The difference between the two emphasizes that the orientation of a receiver has a strong impact on the coupling of interfering light sources. The superimposed measurements are deconstructed (following Algorithm 1) to allow for individual light source modelling. The sources are identified by considering the angle to the measurement device. The derived models of the specific spectrum attenuation for the found light sources can then be used for the composition of the measured spectra. A total of 10 different spectral models are derived that way, each representing a common light source found in the examined sites. In Fig. 6, three of these identified source models are represented as an output of Algorithm 1. The info screen represents human machine interfaces. Occupying a completely different spectrum also a MIG-welding spectrum and that of an optical tracking system is presented. However, when re-composing the measured spectrum with these models, not all measured intensities could be explained. These remains are not clearly relatable and will be factored in by creating a rest model, which averagely takes in 14 % of the total irradiation measured.

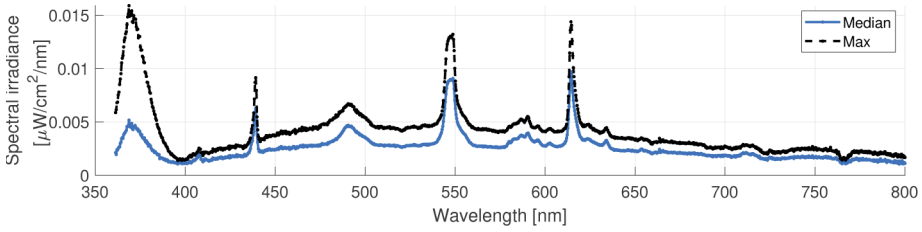

Fig. 5. Exemplary spectral irradiance distribution of a whole spherical measurement

Optics EXPRESS

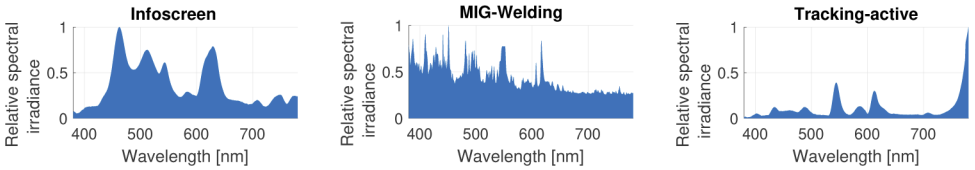

Fig. 6. Normalized irradiance distribution models of different light sources in the industrial environment in the visible spectrum (380 - 780 nm).

By further grouping of these models the occurrence in the lighting composition becomes apparent. Fluorescent lighting and white LEDs represent the apparent artificial illumination. Furthermore, light emitting processes are found, like metal inert gas (MIG) welding or UV based lacquering. In the group human machine interfaces info screens and and a projector model are accumulated. Furthermore, optical tracking systems has been found, exhibiting two different spectra, dependent on the current state of operation. The composition of the found industrial environments can be expressed by the respective portion of these groups as presented in Fig. 7. Whereas in some production environments work is done in 87 % direct sunlight, other locations do not have any sunlight, thus switching between extremes. The artificial illumination portion behaves analogously. On average, the production environment is composed of 33 % artificial lighting, 37 % sunlight, 16 % of light emitting processes and to 14 % of remaining irradiance. The total irradiation of these light sources also varies. The median of the irradiance is 3.8 $\mu W/cm^2$, whereas considerably brighter (17.1 $\mu W/cm^2$) and darker locations (0.9 $\mu W/cm^2$) could also be found. It has been found that the excited wavelength bands also vary from site and location. When accumulated, the whole visible spectrum is occupied by superposition of different, heterogeneous light sources (in accordance to [25]). However, at a specific location, typically only a subset of all possible light sources reach the receiver, leaving certain wavebands open or barely occupied, as can be seen in Fig. 5. In this example, derived from the irradiance maxima (irradiance above 5 $nWcm^{-2}nm^{-1}$) a band of approximately 80 nm is occupied, divided in six sub-bands. In this case, the visible spectrum is barely occupied, opening 320 nm of usable, but discontinuous bandwidth. The optical interference can be suppressed by optical filtering, which needs to be adaptive to the environment. Otherwise, interfering radiance will introduce a dynamic component at the received signal. As previously derived, the flicker in the electrical domain is also measured. For the process of MIG welding the frequency representation of the emitted light intensity is presented in Fig. 8. A light flicker of 75 Hz and 5 MHz can be observed. In contrast, in the grinding process no characteristic flickering is measured. In Fig. 9 in turn, the excitation frequencies of all sites is presented accumulated. Light flickers ranging from 50 Hz up to 65.7 MHz with decreasing intensity. The four strongest excitation frequencies include 50 Hz, 75 Hz, 32.5 kHz and 5 MHz.

The spectrum occupation combined with the accumulated flickering induces interference leading to bit errors. In Fig. 10 the results of different, interfering irradiance levels based on the calculation in Eq. (12) and Eq. (16) are demonstrated. For an irradiation of 10^{-2} $\mu W/cm^2$ the channel capacity is showing differences between noise levels. Up to this point the theoretical channel capacity is solely dependent on the irradiation of the interfering signal. At a noise density of $4 \cdot 10^{-15}$ W/Hz the theoretically achievable channel capacity is limited to 1330 Mbit/s. This effect becomes more pronounced in case of OOK-NRZ modulation as demonstrated in Fig. 10 (right). The data rate is limited to approximately 10 kbit/s in case of interfering irradiation of 0.1 $\mu W/cm^2$ (for $N_0 = 4 \cdot 10^{-15}$ W/Hz). A data rate of 100 Mbit/s is possible if the interfering irradiation is below $I_{int} = 10^{-3}$ $\mu W/cm^2$ and noise density levels of $N_0 = 4 \cdot 10^{-17}$ W/Hz. The frequency characteristic of the interfering light sources is of great importance to the communication performance. The modulation signal should avoid occupied electrical frequencies or optical

Optics EXPRESS

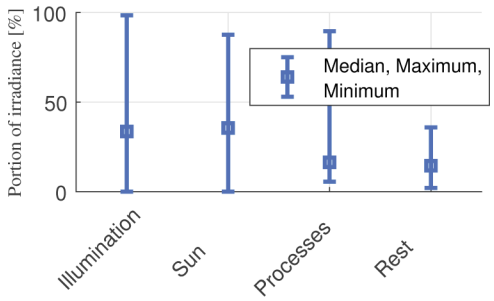

Fig. 7. Portion of different light sources in the production environment for illumination (artificial), the sun, processes and a rest.

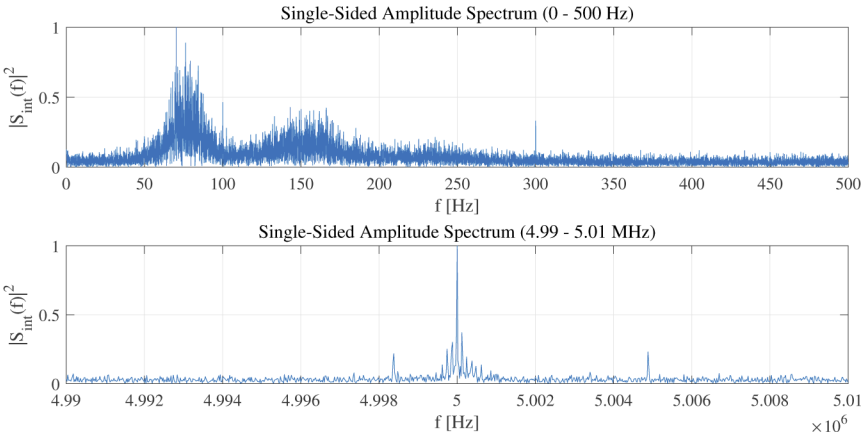

Fig. 8. Frequency spectrum of a MIG welding process at characteristic frequencies (75 Hz, 5 MHz)

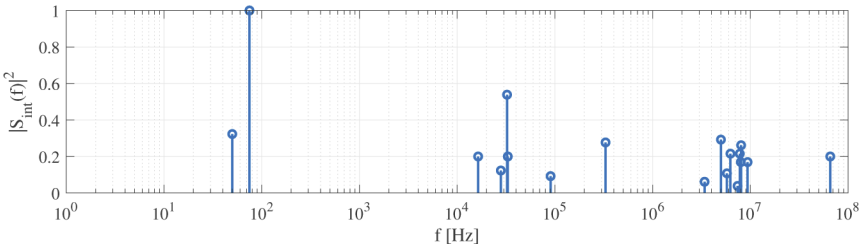

Fig. 9. Frequency spectrum of the environments in total

Optics EXPRESS

wavelength bands. This can be done by an appropriate modulation scheme, which avoids lower frequency components and maybe also particular frequencies. A wavelength-division multiplexing or modulation approach could be suited to prevent such interference. With the gained information it can be derived, that an overall applicable VLC system should be able to adaptive emit and receive light form discrete bands within the spectrum to prevent cross talk.

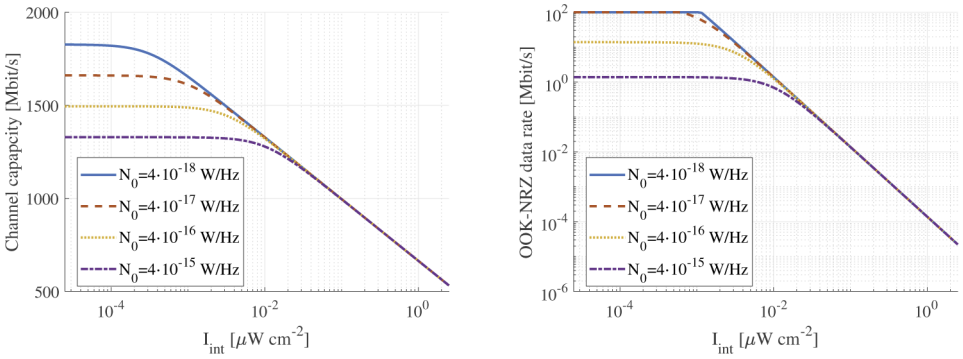

Fig. 10. Simulation results of the influence of interfering irradiance on the theoretical capacity (left) and OOK-NRZ transmission (right) for $BER \leq 10^{-9}$ at different noise spectral densities N_0.

4.3. Multi-path propagation due to reflective surfaces

As mentioned above for the multi-path effect only the reflected signal paths are relevant, not the line of sight. For each of the signal propagation paths, a different average delay τ_k and attenuation α_k can be estimated specifically for an environment [34]. In order to investigate the channel characteristics different methods of channel sounding can be employed, for instance short pulses [35]. A drawback is the generation of sufficient pulse energy to reach long distances. Short pulses have the advantage that they can be measured directly in the time domain to derive the attenuation and delay for a TDL model [35] for example by fitting [28]. The frequency dependent attenuation can be measured by using a swept light signal, but is limited by the light source (LED: max. 10 kHz - 5 MHz in 30 cm distance) [36]. An LED based measurement system therefore has a bandwidth restriction depending on the shortest achievable pulse duration. Furthermore, the radiation pattern of the light emission is a key aspect for the multi-path propagation and VLC performance characteristic. A broader field of view would allow more mobility, while reducing the maximum achievable distance. However, a too short distance would not exhibit the multi-path characteristics because the possible reflections of the beam would not be detected (for the measurement setup an LED array is used, emitting periodic pulses in a divergence angle of 90° in order to measure most of the possible reflected paths). In a static setup, a photo-detector array receives the light pulses in up to 2.8 m distance. In the mobile scenario the transmitter is moved longitudinally to the receiver on a conveyor belt (velocity 0.2 m/s) so that the transmission length changed and could be longer. Comparing realistic scenarios theoretically and experimentally, this worst-case scenario was chosen. The main bandwidth limitation of the reflections can be attributed to the delay differences between the line-of-sight and the longest reflected path, which still contributes significantly to the transmission. The amount of contribution is determined by the attenuation the signal suffers along its way, which be mostly attributed to the reflectivity of the surface and the field of view. In Fig. 11 the setup for the multi-path measurement is shown. No filter or signal processing is used in order to detect most of the multi-path effects. An array of Kingbright L813 LEDs is used. By emitting light pulses through the optical channel, the detected signal is a superposition of the reflected signals portions as illustrated in Fig. 12 (left).

Optics EXPRESS

The first pulse received, serves as a reference to which the attenuation and delay of the following pulses is related. The median of 20 measurements (at the same location in a worst-case scenario) is used to represent the relative averages of power and delay.

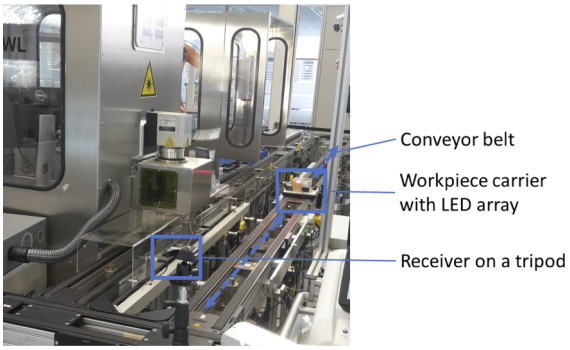

Fig. 11. Measurement setup for worst-case multi-path propagation in an exemplary production environment. This setting was chosen due to the reflective metallic surfaces and glass windows.

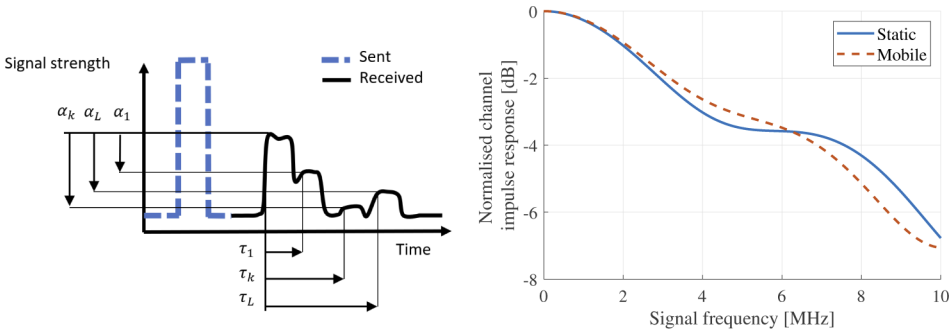

Fig. 12. Measurement data and TDL parameter derivation (left) and frequency responses for measured parameters according to Table 1 (right).

The impulse responses in the industrial environment exhibit the expected multi-path property of delayed and attenuated pulses. In Table 1 the averaged delay and power is listed for the static and mobile scenario. Five taps have been identified who represent the delays ranging from 23 ns to 156 ns with a respective relative attenuation ranging between −3.9 dB to −10.4 dB. The first tap has the biggest impact on the signal and is similar in both the static and the mobile scenarios. This affects the channel impulse response $\underline{H}_e(f)$ according to Eq. (15). In Table 1 the channel response is demonstrated for different modulation frequencies of the signal. In general the mobile scenario does exhibit a very similar behavior compared to the static scenario. Both frequency responses exhibit a low 3-dB bandwidth of approximated 4 MHz, which would restrict OOK-NRZ transmission to data rates below 10 Mbit/s.

5. Discussion

The measurements and the communication model allow the estimation of VLC connection errors due to physical effects in industrial environments. The specific analysis of the three – typically present – physical effects clarify the difference to environments without these effects, like laboratory environments or offices. Although representing a small sample size, it can be

Optics EXPRESS

assumed that most of the production environment exhibit these effects, but differently pronounced. Specifically for each degrading effect the significance is discussed hereafter.

Attenuation due to dust: Outdoor optical wireless communication systems face the weather, which has a considerable effect on the signal in outdoor environments e. g. dense fog is decreasing the signal quality significantly (e. g. up to 80 %) [2,15]. In indoor systems these effects are not to be expected. In turn it has been found that the average particle density in the production environment has also an impact on the communication and it must be differentiated between different types of industries according to the amount of dust of the involved processes. However, this effect is dependent on the modulation scheme, leading to a strong decrease in data rate for OOK-NRZ. Other modulation schemes are to be investigated in future work.

Environmental sources of light: The measured light disturbances pose an enormous time and location-varying noise for a VLC system. The considered intensity distribution diverges from the currently assumed white noise. The introduced analysis method to derive the spectral emission characteristic of individual light sources from superimposed spectral measurements proved to be effective when individual dark room measurements are not viable. 14 % of the measured irradiation, however, could not be modelled and need some further elaboration to gain more precise results. Every examined company has used a variety of lighting devices either out of partial renewal or because of regions with special illumination needs. Especially when color-shift keying is used the receiver typically uses a dedicated optical filter [37,38], or a blue filter is used for bandwidth improvement [39,40].

Whereas this reduces the amount of noise originating from other wavelength bands, the measurements demonstrate environmental noise in the electrical domain will still be present. The often used electrical filtering of the received signal, for example with a high-pass filter, which cuts off the DC components up to 100 Hz [41], will not eliminate the observed flickering effect in every situation. A reliable VLC system therefore needs to be adaptive to the environment in terms of the signal processing and the excited spectrum band.

Multi-path propagation due to reflective surfaces: Multi-path propagation decreases the achievable data rate. The measured TDL model exhibits that mobile and static applications behave about the same. However, the speed of the measured mobile process is relative low, as processes exits, which accelerate objects up to 30 m/s (e.g. transportation drones). In general, the industrial environment poses a considerable multi-path property. In comparison to the standardised ITU radio TDL models, the observed light-based reflections showed lower delay differences, although a worst-case scenario was chosen. This indicates the need of an individual TDL scenario for industrial environments, which accounts for the shorter communication distances and thus also smaller delay differences. The longer and wider the optical beam, the more reflections and signal degradation is to be expected. This signal degradation is severe, leading to a strong decrease of the signal quality.

In summary, it has been shown that common methods for noise reduction by optical and electrical filtering at the receiver may pose ineffective against these types of noise, when not adjusted accordingly. In this study, the environmental light sources show the biggest impact on the communication in most industrial applications and should be tackled. One approach to overcome this issue is to employ an adaptive system, based on a novel wavelength-division multiplexing approach [42], whose results will be discussed in future publications. When combined with the other degrading effects, it is expected that the performance degradation is even more severe. The analysed physical effects could explain the performance reduction of current VLC systems in industrial environments. Whereas the need for reliable wireless communication systems is particularly pronounced in industrial applications, the harsh environment poses a hindrance for most VLC communication systems. It should be noted that the measurements conducted here represent just a probe. These however emphasise how different the dynamic behaviour of light sources are.

Optics EXPRESS

6. Conclusion

This work presents a comprehensive analysis of degrading effects on VLC systems in industrial applications. Empirically, each degrading effect has been analysed at five different production sites. A novel method for deducing the individual spectral emission of superimposed measurements is successfully demonstrated as well as a model to quantify the impact on the communication. Besides industries, which involve a lot of dust or do not apply sufficient ventilation, environmental and artificial light sources seem to have the biggest impact. The limited performance of VLC systems in industrial environments can not only be explained by these effects, but their influence in the electrical and optical domain can be identified and quantified. Thus, they should be considered in the design of a VLC system.

Funding. Deutsche Forschungsgemeinschaft (EXC 2122, ProjectID 390833453); Bundesministerium für Wirtschaft und Technologie (20168 N).

Disclosures. The authors declare no conflicts of interest.

References

1. Cisco, "Cisco annual internet report (2018–2023)," Tech. rep., Cisco Systems (2020).
2. Z. Ghassemlooy, W. Popoola, and S. Rajbhandari, *Optical wireless communications: System and channel modelling with MATLAB* (CRC Press, 2013).
3. D. C. O'Brien, "Visible light communications: Optical wireless communication challenges and potential," *IEEE Photonic Society 24th Annual Meeting* (2011).
4. J. Javaudin, M. Bellec, D. Varoutas, and V. Suraci, "Omega ict project: Towards convergent gigabit home networks," *IEEE 19th International Symposium on Personal, Indoor and Mobile Radio Communications* (2008).
5. D. Karunatilaka, F. Zafar, V. Kalavally, and R. Parthiban, "Led based indoor visible light communications: State of the art," IEEE Commun. Surv. Tutorials **17**(3), 1649–1678 (2015).
6. P. H. Pathak, X. Feng, P. Hu, and P. Mohapatra, "Visible light communication, networking, and sensing: A survey, potential and challenges," IEEE Commun. Surv. Tutorials **17**(4), 2047–2077 (2015).
7. V. Jungnickel, D. Schulz, J. Hilt, C. Alexakis, M. Schlosser, L. Grobe, A. Paraskevopoulos, R. Freund, B. Siessegger, and G. Kleinpeter, "Optical wireless communication for backhaul and access," *European Conference on Optical Communication (ECOC)* (2015).
8. S. M. Verbrugh, E. J. Knibbe, J. W. H. Kuppen, and J. C. A. F. M. Van Gardingen, *Maintaining a lighting system* (Patent WO/2017/021149, 2017).
9. M. Kavehrad, M. I. S. Chowdhury, and Z. Zhou, *Short Range Optical Wireless: Theory and Applications* (Wiley, 2015).
10. D. Schneider, H. Fast, T. Schuba, K. Ferfers, and H. Flatt, "Mobile production - communication in a new light," *Wireless Conference* (2020).
11. P. W. Berenguer, P. Hellwig, D. Schulz, J. Hilt, G. Kleinpeter, J. K. Fischer, and V. Jungnickel, "Real-time optical wireless communication: Field-trial in an industrial production environment," *European Conference on Optical Communication (ECOC)* (2018).
12. S. Riurean, M. Leba, A. Ionica, O. Stoicuta, and C. Buioca, "Visible light wireless data communication in industrial environments," IOP Conf. Ser.: Mater. Sci. Eng. **572**, 012095 (2019).
13. H. Elgala, R. Mesleh, and H. Haas, "Indoor optical wireless communication: Potential and state-of-the-art," IEEE Commun. Mag. **49**(9), 56–62 (2011).
14. A. Sevincer, A. Bhattarai, M. Bilgi, M. Yuksel, and N. Pala, "Lightnets: Smart lighting an mobile optical wireless networks - a survey," IEEE Commun. Surv. Tutorials **15**(4), 1620–1641 (2013).
15. S. Rajbhandari, Z. Ghassemlooy, J. Perez, H. Le Minh, M. Ijaz, E. Leitgeb, G. Kandus, and V. Kvicera, "On the study of the fso link performance under controlled turbulence and fog atmospheric conditions," *Proceedings of the 11th International Conference on Telecommunications* (2011).
16. G. Wypych, *Handbook of Material Weathering* (Elsevier, 2018).
17. D. R. Bates, "Rayleigh scattering by air planetary and space science," Planet. Space Sci. **32**(6), 785–790 (1984).
18. I. I. Kim, B. McArthur, and E. J. Korevaar, "Comparison of laser beam propagation at 785 nm and 1550 nm in fog and haze for optical wireless communications," Proc. SPIE **4214**, 26–37 (2001).
19. H. Hemmati, *Deep space optical communications*, vol. 1 (Wiley, 2006).
20. M. Ilić, I. Budak, B. Kosec, A. Nagode, and J. Hodolič, "The analysis of pbooks emission during the process of grinding of steel en 90mnv8," Metalurgija (2014).
21. H. Horvath, "Atmospheric light absorption-a review," Atmospheric Environ. Part A. Gen. Top. **27**(3), 293–317 (1993).
22. N. S. Kopeika and J. Bordogna, "Background noise in optical communication systems," Proc. IEEE **58**(10), 1571–1577 (1970).

Optics EXPRESS

23. A. Moreira, R. T. Valadas, and A. M. de Oliveira Duarte, "Characterisation and modelling of artificial light interference in optical wireless communication systems, International Symposium on Personal," Indoor and Mobile Radio Communications (1995).
24. A. C. Boucouvalas, "Indoor ambient light noise and its effect on wireless optical links," IEEE Proc. - Optoelectronics **143**(6), 334–338 (1996).
25. D. Schneider, H. Flatt, J. Jasperneite, and O. Stübbe, "Analysis of industrial production environments and derivation of a novel channel model towards optical wireless communication," SPIE Optical Fabrication, Testing, and Metrology VI (2018).
26. J. D. Parsons, *The mobile radio propagation channel* (Wiley, 2001).
27. J. A. Cortés, M. C. Aguayo-Torres, F. J. Cañete, G. Gómez, E. Martos-Naya, and J. T. Entrambasaguas, "Vehicular channels: Characteristics, models and implications on communication systems design," Wireless Pers. Commun. **106**(1), 237–260 (2019).
28. T. S. Rappaport and S. Y. Seidel, "Radio channel models in manufacturing environments," Wireless Information Networks Workshop (1989).
29. ITU, "Guidelines for evaluation of radio interface technologies for imt-advanced: M series, itu-r m.2135-1," Tech. rep., International Telecommunication Union (2009).
30. J. R. Barry, J. M. Kahn, W. J. Krause, E. A. Lee, and D. G. Messerschmitt, "Simulation of multipath impulse response for indoor wireless optical channels," Journal on Selected Areas in Communications (1993).
31. C. Shannon, "A mathematical theory of communication," Bell Syst. Tech. J. **27**(3), 379–423 (1948).
32. J. G. Proakis and M. Salehi, *Digital communications* (McGraw-Hill, 2008).
33. CEN, "Light and lighting - lighting of work places - part 1: Indoor work places, en 12464-1:2011, Tech. rep.," European Committee for Standardization (2011).
34. I. Sen and D. W. Matolak, "Vehicle-vehicle channel models for the 5-ghz band," IEEE Trans. Intell. Transport. Syst. **9**(2), 235–245 (2008).
35. W. Khawaja, I. Guvenc, D. W. Matolak, U. Fiebig, and N. Schneckenburger, "A survey of air-to-ground propagation channel modeling for unmanned aerial vehicles," IEEE Commun. Surv. Tutorials **21**(3), 2361–2391 (2019).
36. S. M. Nlom, A. R. Ndjiongue, and K. Ouahada, "Cascaded plc-vlc channel: An indoor measurements campaign," IEEE Access **6**, 25230–25239 (2018).
37. E. Monteiro and S. Hranilovic, "Design and implementation of color-shift keying for visible light communications," J. Lightwave Technol. **32**(10), 2053–2060 (2014).
38. X. Liang, M. Yuan, J. Wang, Z. Ding, M. Jiang, and C. Zhao, "Constellation design enhancement for color-shift keying modulation of quadrichromatic leds in visible light communications," J. Lightwave Technol. **35**(17), 3650–3663 (2017).
39. K. Richter, S. Aleksic, and C.-A. Bunge, "Estimating the modulation characteristics of white leds by their color temperature," in *Proc. of the ICTON 2018*, (Bucharest, 2018), p. Tu.A2.1.
40. G. Stepniak, M. Schüppert, and C.-A. Bunge, "Advanced modulation formats in phosphorescent led vlc links and the impact of blue filtering," J. Lightwave Technol.. **33**(21), 4413–4423 (2015).
41. T. Adiono, A. Pradana, R. V. W. Putra, and S. Fuada, "Analog filters design in vlc analog front-end receiver for reducing indoor ambient light noise," *IEEE Asia Pacific Conference on Circuits and Systems (APCCAS)* (2016).
42. D. Schneider and R. Lachmayer, *Störungsadaptive, optische Freiraum-Datenkommunikation in Innenräumen* (Patent DE102021201050.4 (patent pending), 2021).